Morphology for Color Images via Loewner Order for Matrix Fields

Bernhard Burgeth[1] and Andreas Kleefeld[2]

[1] Saarland University,
Faculty of Mathematics and Computer Science
66041 Saarbrücken, Germany
{burgeth}@math.uni-sb.de

[2] Brandenburg Technical University Cottbus,
Faculty of Mathematics, Natural Sciences and Computer Science
03046 Cottbus, Germany
{kleefeld}@tu-cottbus.de

Abstract. Mathematical morphology is a very successful branch of image processing with a history of more than four decades. Its fundamental operations are dilation and erosion, which are based on the notion of a maximum and a minimum with respect to an order. Many operators constructed from dilation and erosion are available for grey value images, and recently useful analogs of these processes for matrix-valued images have been introduced by taking advantage of the so-called Loewner order. There has been a number of approaches to morphology for vector-valued images, that is, colour images based on various orders, however, each with its merits and shortcomings. In this article we propose an approach to (elementary) morphology for colour images that relies on the existing order based morphology for matrix fields of symmetric 2×2-matrices. An RGB-image is embedded into a field of those 2×2-matrices by exploiting the geometrical properties of the order cone associated with the Loewner order. To this end a modification of the HSL-colour model and a relativistic addition of matrices is introduced.
The experiments performed with various morphological elementary operators on synthetic and real images demonstrate the capabilities and restrictions of the novel approach.

Keywords: matrix field, tensor field, symmetric matrix, colour images, dilation, erosion, colour space, Einstein addition

1 Introduction

Beginning with the path-breaking work of Matheron and Serra [15, 16] in the late sixties mathematical morphology has provided us with an abundance of tools and techniques to process real valued-images for applications ranging from

medical imaging to geological sciences [14, 17, 18, 20]. Erosion and dilation are the fundamental operations of grey scale morphology relying on the notion of a minimum and a maximum of real numbers. Since minimum and maximum in turn depend on the presence of an order, it is no surprise that morphology for vector valued i.e. colour images does not always provide satisfactory results.
There have been numerous approaches how to extend the mathematical morphology framework to colour or vector-valued images. The main ingredients for such a framework are ranking schemes and the proper notion of extremal operators such as maximum and minimum. Due to the lack of reasonable complete lattice for vectorial data numerous suggestions for ranking schemes (based on various notions of distances, projections, and real-valued transforms) have been made, for a well structured, comprehensive, in-depth, and still up-to-date survey the reader is referred to [2] and the extensive list of literature cited therein. In [10] and [13] a more historic account is presented, while for a study of the background in order theory see [3] and [11]. Depending on the choices made one obtains morphological transforms with specific properties. However, none of these attempts seems to have been accepted unanimously in the image processing community.
Somewhat surprisingly, the situation for (symmetric) matrix valued images is not as hopeless as it might seem at first glance.
Here we consider a (symmetric) *matrix field* F as a mapping

$$F : \Omega \subset \mathbb{R}^d \longrightarrow \mathrm{Sym}(n)$$

from domain $\Omega \subset \mathbb{R}^d$ into the space $\mathrm{Sym}(n)$ of real symmetric $n \times n$-matrices with inner product $\langle A, B\rangle = \mathrm{trace}(AB)$ and (Frobenius-)norm $\|A\| = \sqrt{\langle A, A\rangle}$.
There have been successful attempts to extend the operations of mathematical morphology to images with values in the set of positive definite real symmetric 2×2- or 3×3-matrices [5, 6, 8] since these types of data make a natural appearance in medical imaging as the output of diffusion tensor weighted magnetic resonance imaging (DT-MRI).
The goal of this article is to present an approach to morphological operators for colour images by embedding a colour image suitably into a matrix field. Hence the morphology already developed for matrix fields will give rise to morphology for colour images.

For the coding of a colour image as a matrix field we will make use of a variant of the HSL-colour space and the Loewner order cone for real symmetric 2×2-matrices. This novel concept can be applied to grey value images as well hence it includes scalar (flat) morphology.
The structure of the article is as follows: In Section 2 we present the maximum and minimum operations for matrix-valued data and especially a three-dimensional representation of the Loewner order cone for 2×2- matrices. Section 3 deals with the aforementioned embedding and an operation for symmetric matrices gleaned from the relativistic addition of velocities. We report on results of our experiments with various morphological operators applied to synthetic and real colour images in Section 4. Section 5 we offer concluding remarks and glance at future research.

2 Loewner Ordering: Maximal and Minimal Matrices

The so-called *Loewner order* is a natural partial order on $\mathrm{Sym}(n)$, defined by means of the cone of positive semidefinite matrices $\mathrm{Sym}^+(n)$ by

$$A, B \in \mathrm{Sym}(n): \quad A \geq B :\Leftrightarrow A - B \in \mathrm{Sym}^+(n),$$

i.e. if and only if $A - B$ is positive semidefinite.
This partial order is *not* a lattice order, that is, there is no notion of a unique maximum and minimum with respect to this order [4]. Nevertheless, given any finite set of symmetric matrices $\mathcal{A} = \{A_1, \ldots, A_n\}$, we will be able to identify suitable maximal, resp., minimal matrices

$$\overline{A} := \max \mathcal{A} \quad \text{resp.,} \quad \underline{A} := \min \mathcal{A}\,.$$

Since we will consider images with three colour components we may restrict ourselves from now on to the case of 2×2-matrices in $\mathrm{Sym}(2)$ which offer already three degrees of freedom. The procedure to find these extremal matrices for a set $\mathcal{A}$ is as follows: The cone $\mathrm{Sym}^+(2)$ can be represented in 3D using the bijection

$$\begin{pmatrix} \alpha & \beta \\ \beta & \gamma \end{pmatrix} \longleftrightarrow \frac{1}{\sqrt{2}} \begin{pmatrix} 2\beta \\ \gamma - \alpha \\ \gamma + \alpha \end{pmatrix}, \text{ resp., } \frac{1}{\sqrt{2}} \begin{pmatrix} z - y & x \\ x & z + y \end{pmatrix} \longleftrightarrow \begin{pmatrix} x \\ y \\ z \end{pmatrix}. \qquad (1)$$

This linear mapping creates an isometrically isomorphic image of the cone $\mathrm{Sym}^+(2)$ in the Euclidean space $\mathbb{R}^3$ given by $\{(x, y, z)^\top \in \mathbb{R}^3 | \sqrt{x^2 + y^2} \leq z\}$ and is depicted in Fig. 1(a). For $A \in \mathrm{Sym}(2)$ the set $P(A) = \{Z \in \mathrm{Sym}(2) | A \geq Z\}$ denotes the penumbral cone or penumbra for short of the matrix A. It corresponds to a cone with vertex in A and a circular base in the $x - y$-plane:

$$P(A) \cap \{z = 0\} = \text{ circle with center } (\sqrt{2}\beta, \frac{\gamma - \alpha}{\sqrt{2}}) \text{ and radius } \frac{\mathrm{trace}(A)}{\sqrt{2}}.$$

Considering the associated penumbras of the matrices in $\mathcal{A}$ the search for the *maximal matrix* $\overline{A}$ amounts to determine the smallest penumbral cone covering all the penumbras of $\mathcal{A}$ tightly, see Fig. 1(b). One realises that the height of a penumbra measured from the $x - y$-plane is equal to the radius of its base, namely $\mathrm{trace}(A)/\sqrt{2}$. Hence a penumbra is already uniquely determined by the circle constituting its base. This implies that the search for a maximal matrix comes down to find the smallest circle enclosing the base-circles of the matrices in $\mathcal{A}$. This is a non-trivial problem in computer graphics. An numerical solution for finding the smallest circle enclosing the sampled basis circles has been implemented in C++ by Gärtner [12] and was used in [6] and [8]. However, in our case we employ the implementation of an efficient subgradient method detailed in [22] for the calculation of the smallest circle enclosing them. This gives us the smallest covering cone and hence the maximal matrix $\overline{A}$. To ensure that the base of the penumbra is located in the $x - y$-plane, we will not apply the

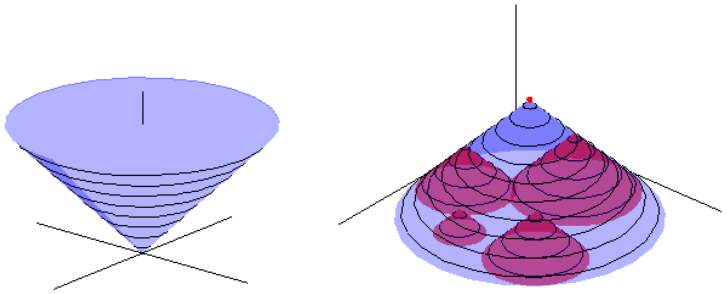

(a) Loewner order cone (b) Covering cone

Fig. 1. Left: Image of the Loewner cone $\mathrm{Sym}^+(2)$. Right: Cone covering four penumbras of other matrices. The tip of each cone represents a symmetric 2×2 - matrix in $\mathbb{R}^3$. For each cone the radius and the height are equal.

above reasoning directly to the matrices $A_1, \ldots, A_n$, but to their shifted versions $\mathcal{A} + \kappa I := A_1 + \kappa I, \ldots, A_n + \kappa I$ with the unit matrix I and the parameter $\kappa := 1/\sqrt{2}$ taking advantage of the relation

$$\overline{\mathcal{A}} = \max(A_1, \ldots, A_n) = \max(A_1 + \kappa I, \ldots, A_n + \kappa I) - \kappa I = \overline{\mathcal{A} + \kappa I} - \kappa I \,.$$

A suitable *minimal matrix* $\underline{A}$ is obtained by means of the formula

$$\underline{A} = \kappa I - \max(\kappa I - A_1, \ldots, \kappa I - A_n)$$

with unit matrix I and the parameter $\kappa = 1/\sqrt{2}$, inspired by the well-known scalar counterpart. For $i = 1, \ldots, n$ we have $\underline{A} \leq A_i \leq \overline{A}$ with respect to the Loewner order. We emphasise that $\overline{A}$ and $\underline{A}$ depend continuously on $A_1, \ldots, A_n$ by their construction. Also the rotational invariance is preserved, since the Loewner order is already rotational invariant: $A \geq B \iff UAU^\top \geq UBU^\top$ holds for any orthogonal matrix U. Nevertheless, the definitions of the matrices $\overline{A}$ and $\underline{A}$ are still meaningful for matrices that are not positive definite as long as they have a non-negative trace (since it corresponds to a radius in the construction above). It also becomes evident from their construction that in general neither $\overline{A}$ nor $\underline{A}$ coincide with any of the A_i: $\overline{A}, \underline{A} \notin \mathcal{A}$.

With these essential notions of suitable maximal and minimal matrices $\overline{A}$ and $\underline{A}$ at our disposal the definitions of the higher morphological operators carry over essentially verbatim.

3 Color Images as Matrix Fields

Closer to the human perception process than the well-known RGB color space is the HSL (or HSI) colour model describing a colour object by its hue, saturation and brightness resp. luminance (see [1, Algorithm 8.6.3] for the conversion).

Replacing in this model the coordinate saturation by the so-called *chroma* leads to a modified version of the HSL-model which we call HC$\tilde{\text{L}}$ colour model. Note that we use this colour model due to its symmetry and its close relation to Ostwald's colour solid (a bicone) from 1916. Of course, other colour models might be applicable.

Its representation is given by a bicone C_2, depicted in Fig. 2(a). To be more

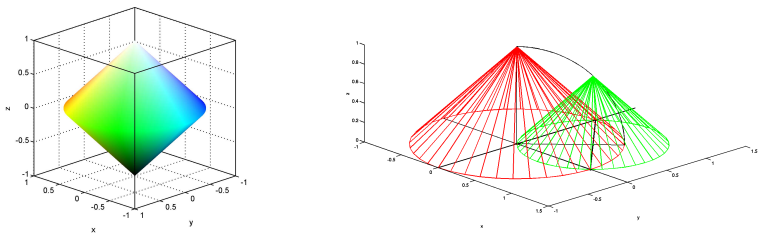

(a) Color bicone (b) The set of maximal and minimal matrices

Fig. 2. Left: HC$\tilde{\text{L}}$-bicone, bicone for the HC$\tilde{\text{L}}$ colour model. Right: The unit ball as the set of extremal matrices stemming from two bicone-matrices.

specific: $\tilde{L} = 2L-1$, for the chroma we have $C = \max\{R,G,B\} - \min\{R,G,B\}$. Hence, any point (x,y,z) of the bicone is coded by $x = C\cdot\cos(2\pi\cdot H)$, $y = C\cdot\sin(2\pi\cdot H)$, $z = \tilde{L}$ providing us with an one-to-one transformation from the HC$\tilde{\text{L}}$ colour space to the RGB colour space. The HC$\tilde{\text{L}}$-bicone corresponds via (1) directly to the order interval $\frac{1}{\sqrt{2}}[-I,I]_L := \{A \in \text{Sym}(2) \,|\, -\frac{1}{\sqrt{2}}I \leq A \leq \frac{1}{\sqrt{2}}I\}$, where the L abbreviates Loewner. In total this establishes the desired continuous one-to-one correspondence of the matrices in $\frac{1}{\sqrt{2}}[-I,I]_L$ with the colours in the HC$\tilde{\text{L}}$ (and from there to the standard RGB space, if so desired),

$$\Psi : \text{HC}\tilde{\text{L}} \subset I\!R^3 \longrightarrow \frac{1}{\sqrt{2}}[-I,I]_L \subset \text{Sym}(2)\,.$$

Exploiting this correspondence one obtains, for example, the maximum of two colours $c_1, c_2 \in \text{HC}\tilde{\text{L}}$ by transforming them into the matrices $\Psi(c_1), \Psi(c_2) \in \frac{1}{\sqrt{2}}[-I,I]_L$, then taking the maximum $\max(\Psi(c_1),\Psi(c_2))$ of these two matrices which is then transformed back to the new 'maximal colour'

$$\max(c_1,c_2) := \Psi^{-1}\left(\max(\Psi(c_1),\Psi(c_2))\right)\,.$$

Ψ^{-1} combines the mapping (1), with the transform into polar coordinates via $H = \frac{1}{2\pi}\text{arg(y, x)}\,, C = \sqrt{x^2+y^2}\,, \tilde{L} = z$, with a principal value of an appropriate argument function. The luminance L is obtained via $L = (\tilde{L}+1)/2$ while the saturation is given by $S = 0$ if $C = 0$, otherwise $S = C/(1-|2L-1|)$.

Having obtained those HSL-values, we convert them to the normalized RGB-values (see [1, Algorithm 8.6.4] for the conversion). The minimum of two colours is treated analogously. Hence by applying this rationale basic morphological operations can be transferred from matrix fields to color images.

However, we are facing two rather severe problems:

1. Elementary geometric reasoning, as indicated in Fig. 2, reveals that the set $\{\max(A,B) \cup \min(A,B) \,:\, A,B \in \frac{1}{\sqrt{2}}[-I,I]_L\} = \mathbb{B}_1$, that is, it equals the unit ball in $\mathrm{Sym}(n)$ visualised as the unit ball in $\mathbb{R}^3$. Hence corresponding HCL- and RGB-values do not exist.
2. Neither $\frac{1}{\sqrt{2}}[-I,I]_L$ nor $\mathbb{B}_1$ are closed under matrix addition, as it is necessary for the design of morphological top-hats or gradients. Again this would entail non-existence of corresponding HCL- and RGB-values.

We overcome the first difficulty by establishing a one-to-one mapping from the bicone C_2 to the unit ball $\mathbb{B}_1$. We begin by defining for a given point $(x,y,z) \in C_2$, a warp factor w by

$$w(x,y,z) = \begin{cases} 1, & \text{if } x,y = 0, \\ \frac{1+\Gamma}{\sqrt{1+\Gamma^2}} \;\text{ with }\; \Gamma = \frac{|z|}{\sqrt{x^2+y^2}}, & \text{otherwise.} \end{cases} \tag{2}$$

Multiplication of point coordinates with its warp factor establishes a one-to-one mapping from C_2 onto $\mathbb{B}_1$ in principle usable for the pull-back of matrices to the color cone C_2. However, experiments reveal that the use of this simple way mapping might lead to a fading of colors and the appearance of a grey tinge as reported in [7]. Instead we define a deforming warping factor

$$w_{\mathrm{deform}}(x,y,z) = 1 + \left(\sqrt{x^2+y^2} + |z|\right)^n \left(w(x,y,z) - 1\right),$$

where $n \geq 1$ is some parameter. Large values of n cause points in the double-cone to remain almost unchanged, while the outer layer is not stretched proportionally. We choose $n = 10$ as it seems to be a large enough value to fit our needs. The mapping w_{deform} has to be inverted numerically by applying a root finding algorithm to

$$t^n - t^{n-1} + 1 - w_{\mathrm{deform}}(x,y,z) = 0$$

for a point $(x,y,z) \in \mathbb{B}_1$. We always apply this inverse mapping (pull-back from $\mathbb{B}_1$ to C_2) after our procedures to find the extremal matrices, and prior the decoding of the matrices into colors.

To resolve the second problem we extend Einstein's general rule for the addition of velocities (see [19, 21]) in the theory of Special Relativity (with speed of light $c = 1$) to symmetric matrices. Einstein's addition in $\mathbb{B}_1$ ensures that we stay inside $\mathbb{B}_1$ (this is our universe). Precisely, let $\alpha_A = \sqrt{1 - \|A\|^2}$ then define the Einstein addition $+_e$ by

$$A +_e B := \frac{1}{1 + \mathrm{trace}(A \cdot B)} \left(A + \alpha_A \cdot B + \frac{1}{1+\alpha_A} \mathrm{trace}(A \cdot B) \cdot A \right).$$

A commutative version $+_{ec} : \mathbb{B}_1 \times \mathbb{B}_1 \longrightarrow \mathbb{B}_1$, the Einstein coaddition (see [21]), reads in this context as

$$A +_{ec} B := \frac{\alpha_A B + \alpha_B A}{\alpha_A + \alpha_B} +_e \frac{\alpha_A B + \alpha_B A}{\alpha_A + \alpha_B} . \tag{3}$$

The corresponding subtraction is given by $A -_{ec} B := A +_{ec} (-B) = -B +_{ec} A$. Hence we can (Einstein-)add and subtract without restrictions in $\mathbb{B}_1$, as it is necessary for many morphological operators.

4 Experimental Results

In this section some elementary morphological operators will be applied to both synthetic and natural colour images of various sizes. In the experiments we use different structuring elements (SE): a cross-shaped structuring element consisting of five pixels ($\mathrm{SE}_{\mathrm{cross}}$), a 3×3-square ($\mathrm{SE}_{3\times3}$), and a 11×11-square ($\mathrm{SE}_{11\times11}$), all centered at the middle pixel. Each of the images is extended by an appropriate layer of mirrored boundary values.
In the first experiments we confirm that our colour-morphological operators applied to image 3(a) in Fig. 3 in principle act as regular morphological operators on black-and-white images. As expected dilation and erosion result in an accurate shift of the inner object front, see Figs. 3(b), 3(c). Note that we surrounded the image by a black box to distinguish between the background of the image and the white background of the article.

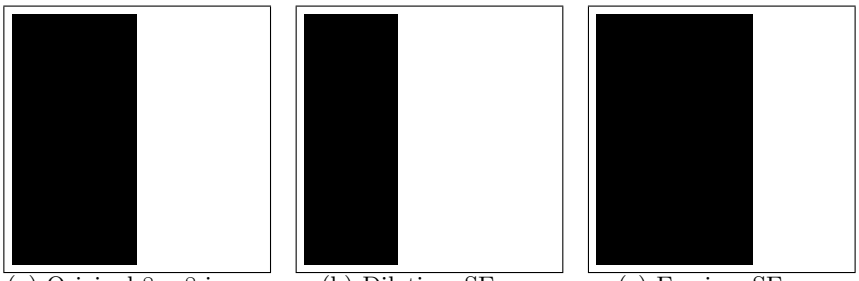

(a) Original 8×8-image (b) Dilation, $\mathrm{SE}_{\mathrm{cross}}$ (c) Erosion, $\mathrm{SE}_{\mathrm{cross}}$

Fig. 3. Dilation and erosion wih $\mathrm{SE}_{\mathrm{cross}}$ applied to bipartite black-and-white image.

Again an image of size 8×8, but with a blue-coloured (RGB= $[0, 0, 255]$) left and a green-coloured (RGB= $[0, 255, 0]$) right is subjected to both a dilation and an erosion. Both colours are located in the $x - y$-plane relatively far apart on the boundary of the $\mathrm{HC\tilde{L}}$ bicone, hence the maximal and minimal matrices are representing white and black respectively. This accounts for the white resp. dark center section in the dilated resp. eroded images in Fig. 4(b) and Fig. 4(d). The component-wise approach produces false colors, as expected, at least

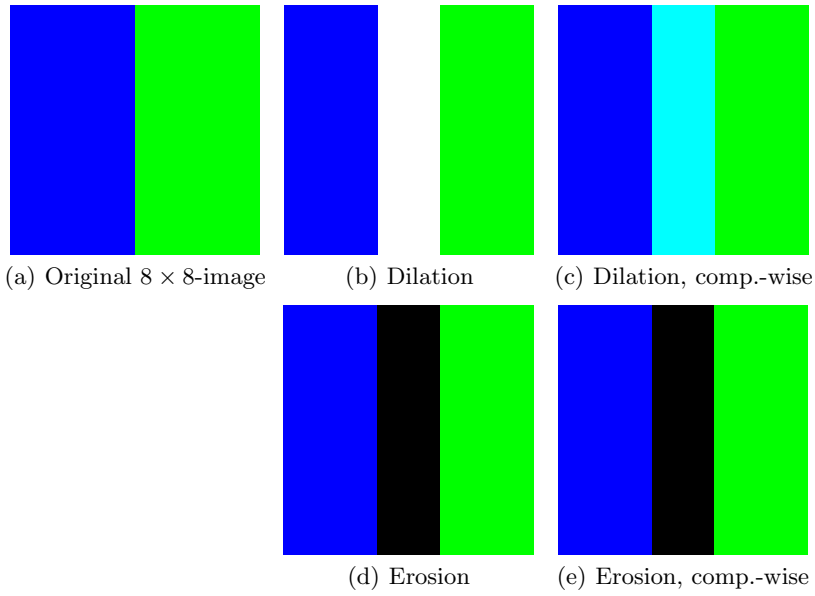

(a) Original 8×8-image (b) Dilation (c) Dilation, comp.-wise

(d) Erosion (e) Erosion, comp.-wise

Fig. 4. Dilation and erosion with $\mathrm{SE}_{\mathrm{cross}}$ applied to bipartite blue-and-green image.

for dilation. Now we consider an RGB-image of resolution 36×24 containing six cross-like structures with the RGB colours $[128, 255, 0]$, $[0, 128, 255]$, $[0, 0, 0]$, $[255, 255, 255]$, $[235, 249, 18]$ and $[249, 155, 18]$ on a red background ($[255, 0, 0]$). Fig. 5(a) shows the constructed image on which a dilation with $\mathrm{SE}_{\mathrm{cross}}$ is applied. In Fig. 5(b) we see the result of the novel matrix-approach, whereas and Fig. 5(c) we see the results of a component-wise approach, namely the dilation of each of the RGB-channels separately. In both approaches the black and white crosses are processed equally well, however, for blue and green cross the channel-wise approach produces clearly false colors, while these crosses get a white halo in the matrix-approach. The next set of experiments employs well-known morphological operators that involve taking the difference of two color images in the matrix setting. We restrict our attention to the self-dual top hat, the Beucher gradient, and the morphological Laplacian. Each operation uses the structuring element $\mathrm{SE}_{\mathrm{cross}}$. Taking the difference here means taking the difference in the sense of the aforementioned Einstein coaddition (3). As expected, in each of the cases the edges of the image objects become prominent, for the morphological derivatives more so than for the top hat. It is also no surprise that all the processed images have a strong grey tinge, the HSL-color close to the equatorial section of the bicone C_2.

It is important to remark that the artefacts in the processed house images are caused by an erroneous top pixel layer that are contained by default in the original image. In grey scale (flat) morphology there is the rule that iterated dilation with a structuring element amounts to the same as applying dilation

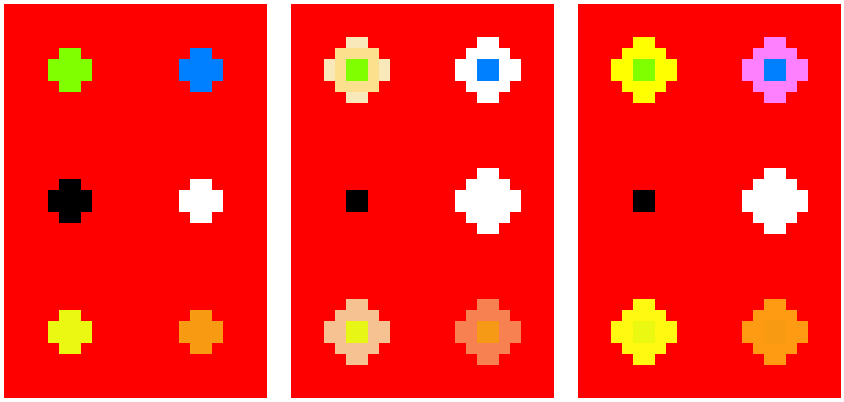

(a) Original (b) Erosion (c) Erosion, comp.-wise

Fig. 5. Erosion with $\mathrm{SE}_{\mathrm{cross}}$ applied to 36×24-synthetic image, in the matrix setting and component-wise.

once with the correspondingly dilated structuring element. For example, 5-fold dilation with a 3×3-square should produce the same result as a single dilation with a 11×11-square. In our matrix-approach this cannot be expected to be the case. We apply to the house image first a dilation with a 11×11-square, then a 5-fold dilation with a 3×3-square. The (Einstein-)difference image is displayed as well in Fig. 7.

We again compare the matrix-approach to the RGB-channel-wise approach, this time for a natural image in the case of the Beucher gradient for a greater effect. In both cases the edge-detecting capabilities of the Beucher gradient are prominent. A difference between the results is noticeable as one can see in Figure 8, but it is now difficult to judge which is better than the other.

Finally note that we did all computation with Matlab on a regular PC. We need 1.1, 4.0, 15.7, 62.2, and 276.2 seconds for a dilation or erosion of an image of resolution 32×32, 64×64, 128×128, 256×256, and 512×512, respectively. Using the profile tool of Matlab reveals that the most time consuming part is needed by the subgradient method to find the smallest enclosing circle of a set of circles. A further speedup will only be possible using C++.

5 Conclusion

Real symmetric 2×2-matrices offer three degrees of freedom. Hence the three components of many popular colour models, such as the RGB- or the HSI-model can be coded as such a matrix. The matrix-setting has indeed several advantages over the vector-setting of colour images: First the algebraic structure is richer, second, there exists a canonical order, the Loewner order, for symmetric matrices. This coding was inspired by the close, almost obvious geometric relation between the $\mathrm{HC\tilde{L}}$ bicone, a variant of the HSI-bicone, and the order

(a) Original (b) Self-dual top hat

(c) Beucher grad. (d) Morph. Laplacian

Fig. 6. Morphological operations with $\mathrm{SE}_{\mathrm{cross}}$ involving differences of images applied to the house-image (with a erroneous color at the top layer of pixels in the original). a) Original, b) self-dual top hat, c) Beucher gradient, d) morphological Laplacian.

interval $\frac{1}{\sqrt{2}}[-I, I]_L$ induced by the Loewner order cone. As soon as the colour image has been rewritten in this way, the morphological techniques developed for matrix fields in [8] and [9] were in principle applicable. However the bicone is not ideal for computations. We used a one-to-one nonlinear mapping to go from the bicone C_2 to the unit ball $\mathbb{B}_1$ in the set of symmetric 2×2 matrices and back, and combined our matrix-valued maximum/minimum operation with it. Standard addition leading to values outside an order interval have been replaced by Einstein coaddition under which $\mathbb{B}_1$ is stable. With these novel techniques various morphological operations ranging from the elementary dilation and erosion to second order derivatives could be studied.

The experimental results are promising and may serve as a proof-of-concept for

(a) Dilation, 11 × 11-SE (b) Dilation, 3×3-SE, 5-fold (c) Difference

Fig. 7. Dilation applied to house-image: a) with 11 × 11-SE, b) with a 3 × 3-SE performed 5 times, c) non-zero difference image (Einstein subtraction).

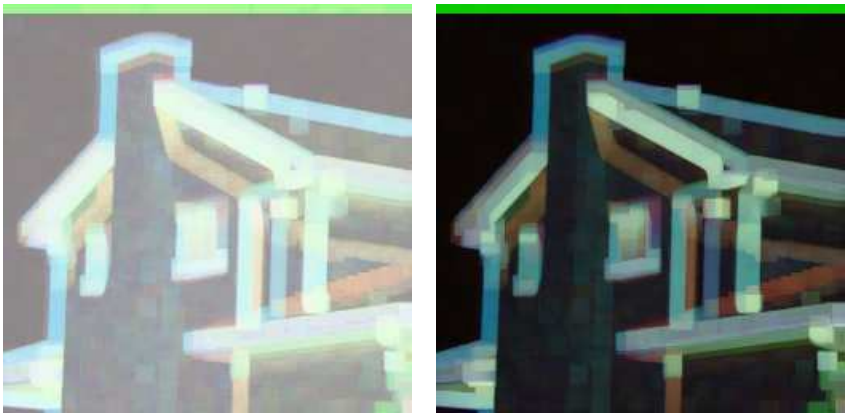

(a) Beucher grad., 11 × 11-SE (b) Beucher grad., 11 × 11-SE, comp.-wise

Fig. 8. Beucher Gradient applied to house-image with 11 × 11-SE, a) matrix setting, b) component-wise.

this novel approach to colour image morphology.
It is clear that the choice of the color cone has a great influence on the results, and in the future will explore other color models as the basis for this approach for color morphology.

References

1. M. K. Agoston. *Computer Graphics and Geometric Modeling: Implementation and Algorithms*. Springer, London, 2005.
2. E. Aptoula and S. Lefèvre. A comparative study on multivariate mathematical morphology. *Pattern Recognition*, 40(11):2914–2929, 2007.
3. V. Barnett. The ordering of multivariate data. *Journal of the Statistical Society*, A 139(3):318–355, 1976.

4. J. M. Borwein and A. S. Lewis. *Convex Analysis and Nonlinear Optimization*. Springer, New York, 2000.
5. T. Brox and J. Weickert. A TV flow based local scale measure for texture discrimination. In T. Pajdla and J. Matas, editors, *Computer Vision – ECCV 2004, Part II*, volume 3022 of *Lecture Notes in Computer Science*, pages 578–590. Springer, Berlin, 2004.
6. B. Burgeth, A. Bruhn, N. Papenberg, M. Welk, and J. Weickert. Mathematical morphology for tensor data induced by the Loewner ordering in higher dimensions. *Signal Processing*, 87(2):277–290, February 2007.
7. B. Burgeth and A. Kleefeld. Order based morphology for color images via matrix fields. In B. Burgeth, A. Vilanova, and C.-F. Westin, editors, *Visualization and Processing of Tensor Fields and Higher Order Descriptors for Multi-Valued Data*. Springer, Berlin, submitted.
8. B. Burgeth, N. Papenberg, A. Bruhn, M. Welk, C. Feddern, and J. Weickert. Mathematical morphology based on the loewner ordering for tensor data. In C. Ronse, L. Najman, and E. Decencière, editors, *Mathematical Morphology: 40 Years On*, volume 30 of *Computational Imaging and Vision*, pages 407–418. Springer, Dordrecht, 2005.
9. B. Burgeth, M. Welk, C. Feddern, and J. Weickert. Mathematical morphology on tensor data using the Loewner ordering. In J. Weickert and H. Hagen, editors, *Visualization and Processing of Tensor Fields*, pages 357–367. Springer, Berlin, 2006.
10. M. L. Comer and E. J. Delp. Morphological operations for color image processing. *Journal of Electronic Imaging*, 8(3):279–289, 1999.
11. E. R. Dougherty (ed.), editor. *Anamorphoses and function lattices*, Mathematical Morphology in Image Processing, New York, 1993. Marcel Dekker. pages 483-523.
12. B. Gaertner. Smallest enclosing balls of points - fast and robust in C++, Last visited: 03.July 2012. http://www.inf.ethz.ch/personal/gaertner/miniball.html.
13. J. Goutsias, H. J. A. M. Heijmans, and K. Sivakumar. Morphological operators for image sequences. *Computer Vision and Image Understanding*, 62:326–346, 1995.
14. H. J. A. M. Heijmans. *Morphological Image Operators*. Academic Press, Boston, 1994.
15. G. Matheron. *Eléments pour une théorie des milieux poreux*. Masson, Paris, 1967.
16. J. Serra. *Echantillonnage et estimation des phénomènes de transition minier*. PhD thesis, University of Nancy, France, 1967.
17. J. Serra. *Image Analysis and Mathematical Morphology*, volume 1. Academic Press, London, 1982.
18. J. Serra. *Image Analysis and Mathematical Morphology*, volume 2. Academic Press, London, 1988.
19. R. U. Sexl and H. K. Urbantke. *Relativity, Groups, Particles: Special Relativity and Relativistic Symmetry in Field and Particle Physics*. Springer, Wien, 2001.
20. P. Soille. *Morphological Image Analysis*. Springer, Berlin, second edition, 2003.
21. A. A. Ungar. Einstein's special relativity: The hyperbolic geometric viewpoint. Conference on Mathematics, Physics and Philosophy on the Interpretations of Relativity, II. Budapest, 2009.
22. S. Xu, R. M. Freund, and J. Sun. *Solution Methodologies for the Smallest Enclosing Circle Problem*. High Performance Computation for Engineered Systems (HPCES), http://hdl.handle.net/1721.1/4015, 2003.